Article

Forces Governing the Transport of Pathogenic and Nonpathogenic *Escherichia coli* in Nitrogen and Magnesium Doped Biochar Amended Sand Columns

Katherine Quinn [1], Sohrab Haghighi Mood [2], Elizabeth Cervantes [3], Manuel Garcia Perez [2,4] and Nehal I. Abu-Lail [1,*]

[1] Department of Biomedical Engineering and Chemical Engineering, University of Texas San Antonio, San Antonio, TX 78249, USA
[2] Department of Biological System Engineering, Washington State University, Pullman, WA 99164, USA
[3] Department of Chemistry, University of Texas San Antonio, San Antonio, TX 78249, USA
[4] Bioproducts Sciences and Engineering Laboratory, Richland, WA 99354, USA
[*] Correspondence: nehal.abu-lail@utsa.edu; Tel.: +1-210-458-8131

Abstract: Background: Access to safe drinking water remains a global issue with fecal indicator bacteria being major pollutants. Biochars offer low-cost adsorbents for bacterial pathogens. A fundamental understanding of how biochars interact with bacterial pathogens is essential to designing effective biofilters. Methods: Water-saturated sand columns amended with Magnesium and Nitrogen-doped biochars produced by pyrolysis at 400, 500, 600, and 700 °C were used to Quantify the transport of pathogenic *Escherichia coli* O157:H7 and nonpathogenic *E. coli* k12 strains in porous media. Measured data were modeled using DLVO theory of colloidal stability. were explored. Results: (1) Biochar is hydrophobic while sand and bacteria are hydrophilic; (2) all Gibbs free energy values quantified between *E. coli* O157:H7 and biochar were negative except for biochar produced at 700 °C; (3) all types of forces investigated (van der Waals, electrostatic, and acid-base interactions) played a role in governing the interactions between bacteria and biochar. Conclusions: (1) Adding doped biochar to sand at a 2% weight ratio enhanced the retention of bacterial cells in the sand/biochar columns; (2) bacterial transport is strain-dependent and mediated by various types of forces resulting from interactions between the various functional groups displayed on bacteria and biochar/sand. Our findings emphasize the importance of monitoring biochar's functionality to eliminate bacterial pollutants from contaminated water.

Keywords: biochar; DLVO; *E. coli*; Gibbs free energy; hydrophobicity; and surface potential

1. Introduction

Today, access to safe drinking water remains a significant issue around the globe. According to the United States Environmental Protection Agency (EPA), urban stormwater, which accounts for just 3% of US land, pollutes 13% of river systems, 18% of streams, and 32% of estuaries surveyed [1]. Many contaminants are present in urban stormwater, including suspended particles, nutrients, heavy metals, hydrocarbons, and, most significantly, bacterial pathogens. Waterborne pathogens in urban stormwater pose a substantial threat to public health worldwide because of the diseases they may cause. Animal waste and on-site waste management systems, such as septic tanks, are significant sources of fecal-derived bacteria found in this stormwater [2].

Fecal indicator bacteria (FIB) are thought to be the major pollutants inhibiting downstream drinking and stormwater usage and are associated with a higher risk of waterborne infections *via* recreational and dietary exposures. Because indicator microorganisms are effective predictors of pathogen prevalence, fecal soil, water pollution, and transport, investigations are often conducted using indicator species such as *E. coli* [3].

Biochars produced by pyrolysis are gaining popularity as low-cost adsorbents for environmental pollutants [4]. Although alternative materials may achieve better removal rates than char, the inexpensive cost, plentiful availability, and potential for land reuse have prompted research in char-based adsorbents [5,6]. Organic matter used in biochar production may originate from a diverse array of feedstock sources. The US has access to over 1.3 billion tons of biomass per year for bioenergy production, mainly maize, wheat, and forestry residues [7,8]. The original biomass structure will influence the subsequent biochar structure, physical properties, and future interactions with other constituents.

Applying biochar to natural porous media (like sand) improves pathogen's retention [2,9–11]. Attachment to and detachment from sand (collector) surfaces and physical entrapment (straining) in confined pore spaces are mechanisms for controlling the retention of microbes and colloids in porous media. Such colloidal interactions with solid surfaces are explained in part by the Derjaguin–Landau–Verwey–Overbeek (DLVO) theory. According to the DLVO theory, interaction energy can be quantified as the sum of van der Waals and electrostatic double-layer interactions [12]. These interactions are affected by a variety of physical and chemical factors [12]. The size of biochar particles, their physical and chemical surface properties, as well as the micro-and macro-porous features of their surfaces are expected to influence bacterial retention in biochar-modified porous media [12]. Packed column experiments are commonly utilized to analyze porous media's colloid breakthrough curves (BTCs) and retention characteristics [12].

Although some column studies were undertaken to explore bacterial's mobility in porous biochar-modified media, little is known about the fundamental mechanisms that govern biochar's efficacy in removing bacteria. Changes in biochar's physical and chemical characteristics may alter bacterial removal capabilities [3,7,13,14]. As such, it is critical to quantify how biochar's morphological and chemical qualities influence its interactions with bacteria and ultimately bacterial transport in sand [7,15].

This study aims at exploring the fundamental mechanisms through which biochar controls the retention of pathogenic bacteria in sand. To achieve this, the physiochemical characteristics of magnesium and nitrogen-doped biochars generated by pyrolysis at four different temperatures (400, 500, 600, and 700 °C), the properties of sand, pathogenic *E. coli* O157:H7, and nonpathogenic control *E. coli* k12, were investigated. After that, the forces that govern the interactions of these various biochars with the bacterial strains were quantified. A discussion of how such forces can inform the design of effective biofilters was included.

2. Materials and Methods

2.1. Model Bacterial Cultures

Pathogenic *E. coli* O157:H7, ATCC 35150 and nonpathogenic *E. coli* k12, ATCC 10798 were used as model bacteria. *E. coli* were activated and harvested as previously described [16]. For details, please refer to section S1 of the supporting information.

2.2. Biochar's Preparation

Avicel cellulose biochars were produced and characterized according to details reported elsewhere [17–19]. Characteristics of biochars are briefly summarized in Table 1. In our previous paper [16], we proved that the oxidation of biochar resulted in the reduction of the capacity of biochar to adsorb *E. coli*. We hypothesized that the negative charge of the oxidized biochar in the range of the pH investigated was responsible for enhancing the electrostatic repulsion between *E. coli* and the biochar leading to a reduced biochar's efficacy. To test this hypothesis and to improve the biochar retention of *E. coli*, we decided to dope the biochar with N-Mg because these biochars are positively charged in a wide pH range and as such will attract *E. coli*, leading to higher retention. For brief descriptions of how biochar was prepared and characterized, please refer to Sections S2 and S3 of the Supporting Information.

Table 1. A summary of the physiochemical characteristics of biochar types pyrolyzed at different temperatures [&].

	Pyrolysis Temperature (°C)			
Physiochemical characteristic	400	500	600	700
Carbon content (wt. %) (dry basis)	64.0	63.6	67.9	63.6
Nitrogen content (wt. %) (dry basis)	8.3	7.7	7.7	11.0
Hydrogen content (wt. %) (dry basis)	4.6	3.2	1.9	1.2
Oxygen content (wt. %) (dry basis)	11.6	11.5	7.1	7.7
Fixed carbon content (wt. %) (dry basis)	54.7	60.2	65.7	64.6
Volatile matter content (wt. %) (dry basis)	33.8	25.8	18.8	18.9
Ash content (wt. %) (dry basis)	11.5	14.0	15.4	16.5
Moisture content (wt. %) ** (as received)	9.2	10.0	6.3	6.0
SA-CO_2 (m^2 g^{-1}) *	202.7	299.8	400.9	493.8
V_{micro} (cm^3 g^{-1}) [&]	0.081	0.120	0.161	0.198
P_{cap} ($cm^3 g^{-1}$) [#]	24.2	26.6	26.9	26.5
Bulk density (g cm^{-3})	1.56	1.551	1.537	1.561
porosity (*v/v*)	0.69	0.60	0.67	0.63
pH (in H_2O)	10.1	10.0	10.0	10.2
Mean particle diameter (μm)	51	32	26	29
Sphericity (%)	0.49	0.49	0.49	0.53

* SA-CO_2 is the surface obtained by adsorption of CO_2 to biochars, [&] V_{micro}: Volume of micro-sized pores within the biochar, and [#] P_{cap}: Total pore capacity. ** Moisture acquired from the air during storage. [&] Currently pending publication elsewhere.

2.3. Sand as a Model Porous Medium

Given the large pore size, sand was our choice of mineral to work with. Industrially manufactured fine quartz sand was used (J.t Backer VWR, Arlington Heights, IL, USA). To quantify the size of the sand particles, images of the sand particles were captured on a glass slide using an Invitrogen™ EVOS™ XL Core Imaging System (Thermo Fischer Scientific, Waltham, MA, USA) at 4X and 10X. Images were saved as a joint photographic group (Jpg). The ImageJ software was used to process the images to quantify the perimeter of individual sand particles. The average diameter of sand particles was 411 ± 66 μm (n = 52) and the sphericity was 0.7 ± 0.1. Represented images of the sand and biochar, along with selected characteristics of the sand, can be found in Supporting Information Section S4, Figure S1, and Table S1.

2.4. Quantification of Bacterial Transport in 2% Biochar/Sand Columns

Thirty-six experiments were conducted to quantify the transport of *E. coli* in biochar-amended sand columns. Three types of porous media were used: (1) the four types of biochar doped with magnesium and nitrogen, (2) sand alone, and (3) 2% of each of the four biochars mixed with 98% sand. Prior to use, the sand was cleaned by washing it with deionized water (DIW) five times to remove any residual fine particles. The sand was then allowed to boil to remove any air bubbles and any extra fine particles. An optical density at a 600 nm wavelength (OD600) of 0.0 of water soaking the sand was indicative of no turbidity. The clean sand was mixed with the biochar at a 98% sand to 2% biochar ratio and dry-packed in short columns. The mixture was saturated with DIW overnight and a cotton ball was placed on the mixture's top to help contain the biochar. Packed columns were acclimated to DIW for at least 10 pore volumes (PVs) (1 PV = 3.6 ± 0.1 mL). Water was pumped into the column using a Fischer scientific GP1100 Precision Variable-Speed Peristaltic Pump (NH, USA). The absorbance of the effluent was measured to determine equilibrium. The bacterial suspension was then pumped upward to avoid channeling in the column at 3.2 mL/min for at least 10 PVs, followed by 5 PVs of bacterial-free medium to elute all cells that may not have been retained in the porous media. A total of 3.2 mL fractions of the effluent were collected using a fraction collector (GE Frac 920, Cytiva, MA, USA), and the absorbance of each fraction was measured. Bacterial outlet concentration

(C) divided by the bacterial inlet concentration (C$_o$) was graphed *vs.* the PV to create the breakthrough curves (BTCs). Each column experiment was repeated 3 times.

2.5. Contact Angles Measurements and Modeling

Contact angles of sand, biochar, and bacteria were measured using the sessile drop method with a drop shape analyzer DSA100 (KRŰSS, Hamburg, Germany). For details on measurements and modeling, please refer to Section S5 and Table S2 of the Supporting Information.

2.6. Interfacial Net Gibbs Free Energy Calculations

The net free Gibbs free energy of adhesion (ΔG_{Adh}) for two interacting surfaces at equilibrium and in contact can be described as a function of apolar and polar free energies. Free energies are related to the surface tension components of the two surfaces estimated from contact angle measurements. The various surface tension components of the bacterial cell, sand, biochar, and solution can be calculated using Equations (S4)–(S12) described in Supporting Information Section S6.

Once all the surface tension components are computed, the Gibbs free energy of adhesion can be calculated using Equation (1). A negative Gibbs energy indicates favorable attachment.

$$\Delta G_{Adh} \frac{mJ}{m^2} = [\gamma_{CS} - \gamma_{CW} - \gamma_{SW}] \tag{1}$$

2.7. Derjaguin, Landau, Verwey, and Overbeek (DLVO) Theory of Colloidal Stability

The initial adhesion of bacteria to a surface was suggested to be controlled by electrostatic and van der Waals interactions, as could be modeled by the classical Derjaguin–Landau–Verwey–Overbeek (DLVO) theory of colloidal stability. According to DLVO theory, the total nonspecific energies (E_{DLVO}) are the summation of the electrostatic energies (E_e) and Lifshitz–van der Waals energies (E_{LW}), as shown by Equation (2) [20].

$$E_{DLVO} = E_e + E_{LW} \tag{2}$$

To generate E_{DLVO} energy profiles, the bacterial cell, biochar, and sand were all considered as spherical particles. The average diameter of the biochar particles generated at different pyrolysis temperatures, as well as the diameter for sand as determined from images, are listed in Table S1. The bacterial diameter was taken as 1.16×10^{-6} m [16]. To calculate the electrostatic energies (E_e, J), a linearized version of the Poisson–Boltzmann expression, as described by Equations (S13)–(S15), was used. In addition, the van der Waals interaction energy (E_{LW}) between two dissimilar spheres can be calculated using a Hamaker expression, and corrected for retardation effects [20] as shown in Equation (S16) in Section S7 in the Supporting Information.

2.8. Statistics

Reported error bars indicate the standard deviation unless mentioned otherwise. Variations or similarities amongst different groups of data estimated for the biochars pyrolyzed at different temperatures were assessed via different means. First, a one-sample *t*-test was used to compare data points in a single group if the normality Shapiro–Wilk test was passed. The non-parametric group comparisons Mann–Whitney rank sum test was used to compare two groups. When multiple groups were compared, the Kruskal–Wallis one-way analysis of variance (ANOVA) was used. If pairs within a group were to be compared, the pair-wise multiple comparison procedure (the Tukey test) was used. In all tests, the power of the tests was taken with α as equal to or less than 0.05 or 95% confidence. Statistically different results indicate that the differences in medians of two groups are greater than would be expected by chance. All tests were done using Sigma Stat 11.1.0.102 (SYS stat Inc.). When data was fit to various models, the quality of the regression fit was judged based on the estimated values of the coefficient of determination (R^2). The closer the R^2 value to 1, the better the fit.

3. Results and Discussion

3.1. Effects of Biochar Pyrolysis Temperature on Bacterial Transport in Porous Media

Figure 1 shows the BTCs of the transport of *E. coli* O157:H7 and *E. coli* k12 through sand mixed with biochars (400, 500, 600, and 700 °C) at a 2 wt. % ratio. The transport of both bacterial strains in negative controls of cotton balls and 100% sand columns were also quantified. The shapes of the BTCs differed depending on the biochar used and the bacterium examined. For example, Figure 1A,B demonstrated symmetrical BTCs with a reasonably sharp breakthrough front, sharp tailing, and a period of constant steady-state adsorption of bacteria to porous media, as indicated by the plateau between pore volumes 6–12 for cotton balls and 10–20 for sand. Such BTCs indicate that the rates of attachment and detachment of bacteria from the sand or cotton balls are similar. They also indicate that the attachment, if any, is irreversible and strongly bound to porous media. In comparison, Figure 1C–F represented asymmetrical BTCs that are exhibiting a degree of tailing in their front adsorption and desorption portions of data. They were also characterized by a continuous slope in the adsorption data that does not establish a steady state during the time of measurements.
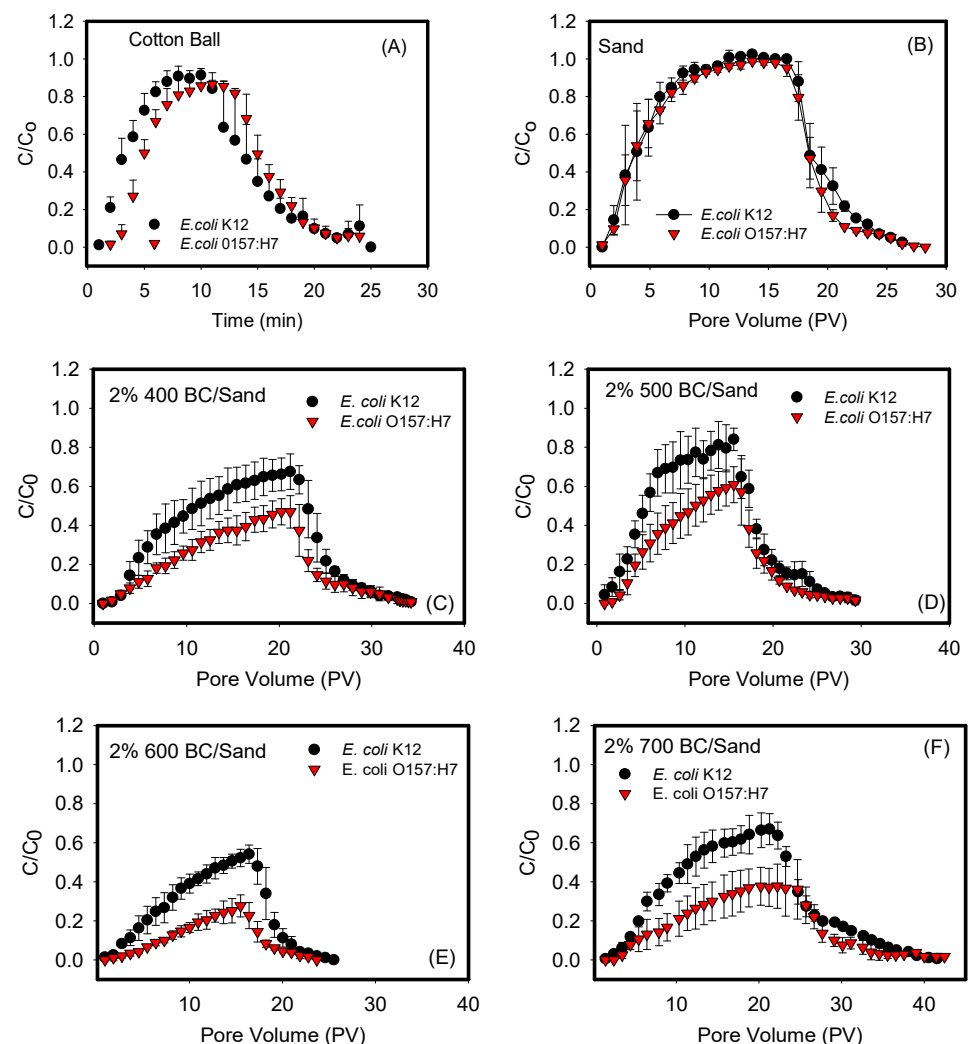

Figure 1. Breakthrough curves (BTCs) for negative controls: (**A**) cotton ball, (**B**) sand, and (**C–F**) biochars 400, 500, 600, and 700 °C. Each curve represents a triplicate with error bars representing the standard deviation. Data shown in (**A–C**) quantified between cotton, sand, and biochar 400 and each of the two bacterial strains were statistically similar with *p* values of 0.984, 0.268 and 0.061, respectively. Data shown in (**D–F**) quantified between biochars 500, 600, and 700 °C and each of the two bacterial strains were statistically different with *p* values of 0.038, 0.017, and 0.024, respectively.

3.2. Net Gibbs Free Energy Calculations

The surface tensions and Hamaker constant listed in Table S2, and the contact angles listed in Table S3 were used to quantify the Gibbs free energies acting between *E. coli* O157:H7 and k12 strains and sand/biochar in water (ΔG) (Figure 2). They were also used to quantify the DLVO energies reported in Section 3.3. A negative value of ΔG indicates a spontaneous favorable process [14]. Differences in system Gibb's energy caused by bacterial adhesion are attributed to interfacial surface tensions. A bacterial strain is hydrophilic to the liquid from the viewpoint of surface thermodynamics if $\Delta G > 0$ and hydrophobic if $\Delta G < 0$ [21,22]. The hydrophilicity increases with the increase of ΔG for $\Delta G > 0$ and the hydrophobicity increases with the decrease of ΔG for $\Delta G < 0$. The explanations above also refer to silica sand [21]. The similarities in the hydrophilicities of sand and *E. coli* account for the favorable Gibbs free energy numbers as seen in Figure 2.
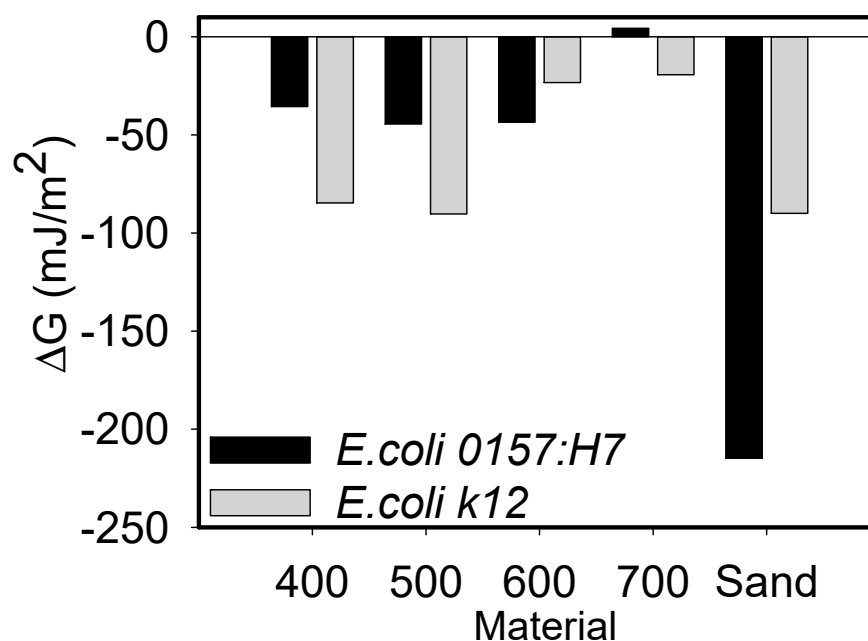

Figure 2. Comparison of the Gibbs free energies calculated for both bacteria strains and biochar types (400–700 °C) or sand in DIW. No statistical differences were measured between the various biochars and bacterial strains investigated.

As can be seen from Figure 2, all quantified ΔG values were negative, except for those quantified between *E. coli* 0157:H7 and biochar 700 °C in DIW where the value was slightly positive (statistically similar, $p = 0.082$). Acid-base Lewis type Gibbs free energy magnitudes calculated between *E. coli* k12 and biochars 400, 500, and 700 °C were more negative compared to those calculated for *E. coli* O157:H7, indicating more favorable interactions for the former (statistically similar, $p = 0.066$). On the contrary, ΔG magnitudes were more negative between *E. coli* O157:H7 and biochar 600 °C and sand compared to *E. coli* k12. It has to be noted that Gibbs free energies account for only a subset of all possible forces that may bring bacteria and biochar or sand together. Other forces that may play a role include DLVO forces; these will be calculated in Section 3.3. Our results are similar to other studies [23].

3.3. Non-Specific, Long-Range DLVO Interactions

The non-specific long-range DLVO interaction energies expected between bacterial strains and biochar or sand in DIW were calculated. Figure 3 shows the electrostatic, van der Waals, and total energy profiles for *E. coli* k12, while Figure 4 shows these for *E. coli* O157:H7. When individually considered, the van der Waals energies acting between *E. coli* k12 and sand and biochars 400, 500, and 600 °C were all repulsive as indicated by the

positive energy values. On the contrary, these interactions were attractive with biochar 700 °C as indicated by the negative energies. Similarly, when the electrostatic energies were considered, the interactions with *E. coli* k12 were all repulsive (sand and biochars 400, 600, and 700 °C). They were attractive with biochar 500 °C.
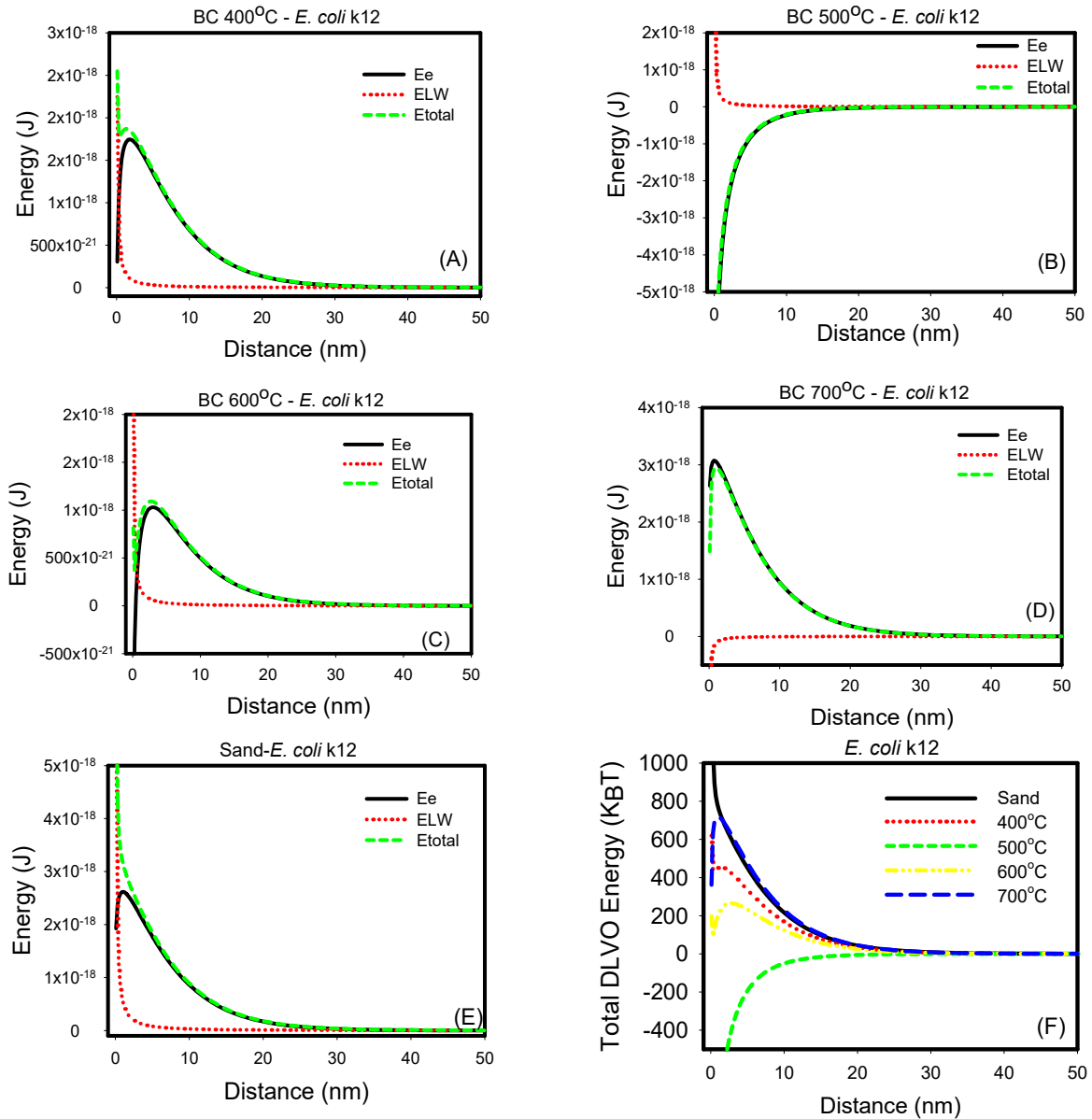

Figure 3. (**A**–**E**) Electrostatic, van der Waal and total energy profiles as a function of distance for interactions between *E. coli* k12 and biochars 400, 500, 600, and 700 °C and sand in DIW. (**F**) Comparison of all total energy profiles between *E. coli* k12 and all biochars and sand in water. The total energy profiles quantified between biochars and *E. coli* k12 were statistically different ($p < 0.001$).
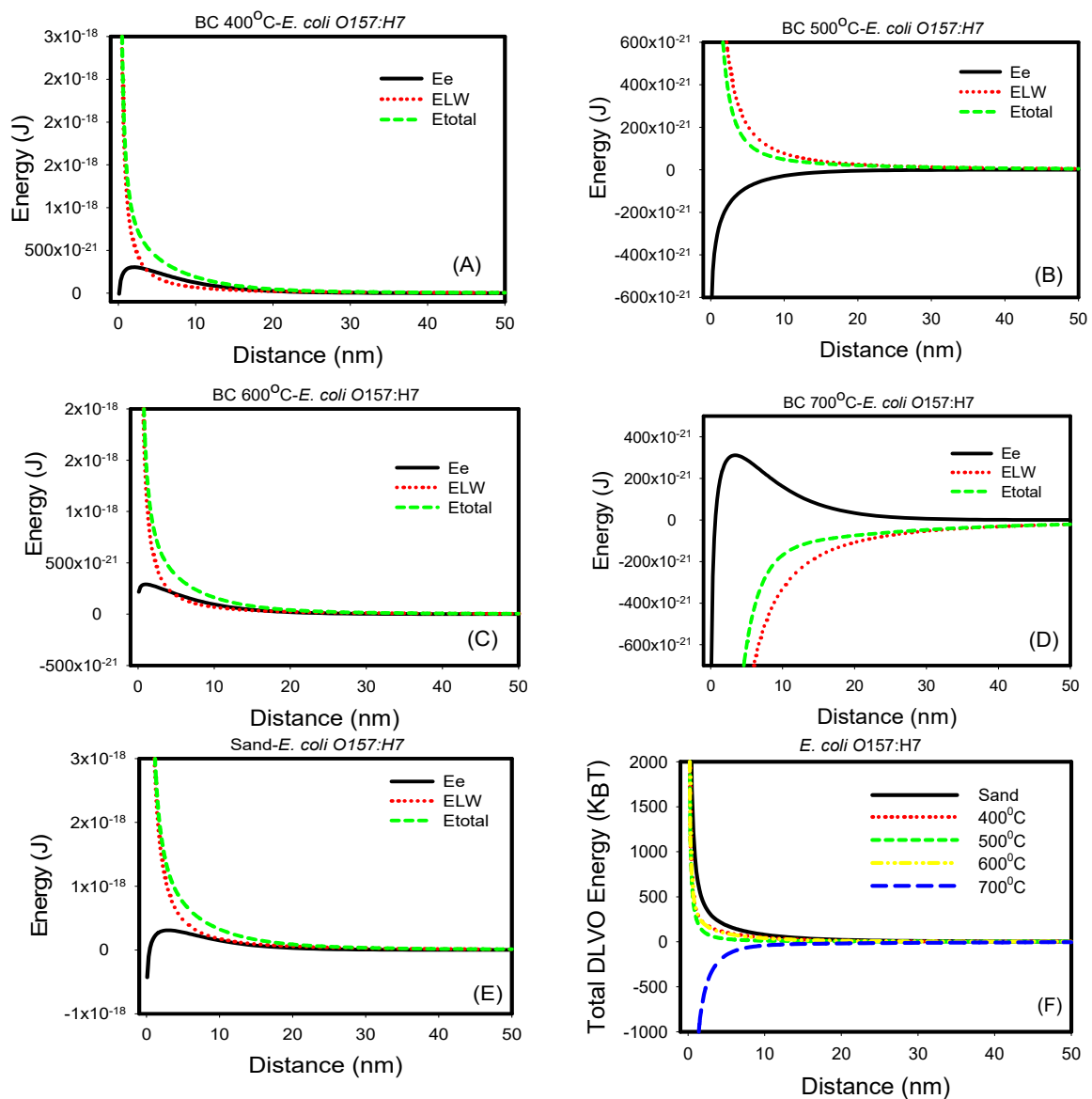
Figure 4. (**A–E**) Electrostatic, van der Waal and total energy profiles as a function of distance for interactions between *E. coli* O157:H7 and biochars 400, 500, 600, and 700 °C and sand in DIW. (**F**) Comparison of all total energy profiles between *E. coli* O157:H7 and all biochars and sand in water. The total energy profiles quantified between biochars and *E. coli* O157:H7 were statistically different ($p < 0.001$).

When the two energy components were compared to each other, it was shown that electrostatic energies dominate over van der Waals energies. Finally, when the total energy profiles were compared for sand and four types of biochar, it was shown that interactions with biochar 500 °C were attractive and thus favorable. Interactions to sand and biochars 400, 600, and 700 °C all showed an energy barrier to be overcome in order for interactions to occur. This energy barrier was beyond the primary minimum for the sand and could not be quantified, indicating that *E. coli*'s k12 attachment to sand is not favorable. Energy barriers between *E. coli* k12 and biochars 400, 600, and 700 °C were 619, 265, and 717 kBT, respectively.

Similarly, when individually considered, the van der Waals energies acting between *E. coli* O157:H7 and sand and biochars 400, 500, and 600 °C were all repulsive as indicated by the positive energy values. On the contrary, these interactions were attractive with biochar 700 °C as indicated by the negative energies. Correspondingly, when the electrostatic energies were considered, the interactions with *E. coli* k12 were all repulsive. When the

two energy components were compared to each other, it was shown that van der Waals energies dominate over electrostatic energies, opposite to what we have seen with *E. coli* k12. This could be attributed to acid-base hydrophobic interaction forces, which could lead to specific forces [24]. Finally, when the total energy profiles were compared for sand and four types of biochar, it was shown that interactions with biochar 700 °C were attractive and thus favorable. Interactions to sand and biochars 400, 500, and 600 °C all showed an energy barrier beyond the primary minimum for interactions to occur, indicating that attachments between *E. coli* O157:H7 and these porous media are not favorable. Our results are similar to other studies [25,26].

Since the size of bacterial cells falls within the spectrum of colloidal particles, the DLVO theory of colloidal stability can be used to model the forces/energies involved in bacterial adhesion processes [24]. According to this theory, the overall interaction forces/energies acting between bacterial cells and a surface are made up of Liftshitz–van der Waals and electrostatic forces. The attraction of van der Waals forces is normally independent of the pH or the ionic strength of the encompassing solution. These interactions are primarily influenced by the Hamaker constant (H_{132}) as detailed earlier [24,27]. H_{132} for biochar 700 °C was positive (7.498×10^{-21} J); it was negative for all other biochars. Similar to biochar 700, Xu et al. quantified positive Hamaker constants for their biochars [28]. Because living cells have a typical diameter of several microns and are surrounded by a plasmid membrane that generates electro-dynamic interactions, DLVO can help predict cellular adhesion, but it is not perfect. DLVO can explain both weak and strong adhesions, and cellular surfaces are mostly negatively charged; however, it lacks the effect of roughness as cells cannot be considered smooth surfaces. The precise distribution of charge in the cell is unknown and the molecules' conformation is not accounted for [29].

The DLVO model cannot thoroughly describe bacterial adhesion. Because of this, van Oss proposed an "extension" of the DLVO theory where the hydrophobic/hydrophilic interactions (as illustrated by the polar ΔG_{AB} part of the surface energy) can be also accounted for. The total adhesion energy can be conveyed as: $E_{DLVO} = E_e + E_{LW} + E_{AB}$, where E_{LW} and E_e are the "classical" van der Waals and double layer interactions and E_{AB} is the acid-base interactions [22,30]. According to van Oss, the latter constituent represents the attractive hydrophobic interactions and repulsive hydration effects, which are typically 10–100 times stronger than the van der Waals interactions of surfaces in primary interactions [22]. The distance dependence is vital in the calculation of the total adhesion energy. The distance dependency is critical in determining overall adhesion energy. The classical DLVO model offers the distance dependency of the double layer and van der Waals interactions, and the surface energy variable E_{AB} decays exponentially from its value at close contact [26]. It should be mentioned that both the E_e and the E_{AB} decrease exponentially, but with varying lengths [27].

4. Conclusions

Amending sand with 2% biochar improved the attenuation of *E. coli* k12 and *E. coli* O157:H7 by an average of 33% and 55%, respectively. This improvement was heavily reliant on the physiochemical properties of biochar and the bacterial strain investigated. All the variations in the physiochemical properties made the transport of the bacterial strains in sand mixed with biochar and the interactions quantified between sand and biochar dependent on the biochar type.

Our DLVO analyses indicated that van der Waals energies dominated over electrostatic energies when *E. coli* O157:H7 was concerned, and the opposite was true when *E. coli* k12 was concerned. Our results also indicated that all Gibbs free energy values quantified between *E. coli* O157:H7 and biochar were negative except for those quantified with biochar 700 °C in DIW where the value was slightly positive. The Gibbs free energy magnitudes calculated between *E. coli* k12 and biochars 400, 500, and 700 °C were more negative compared to those calculated for *E. coli* O157:H7, indicating more favorable interactions for the former. On the contrary, ΔG magnitudes were more negative between *E. coli* O157:H7

and biochar 600 °C and sand compared to *E. coli* k12. Our findings indicate that various forces (van der Waals, electrostatic, and acid-base interactions) may contribute to the regulation of bacteria-biochar interactions. Thus, while designing efficient biochar filters, it is necessary to examine the effects of all of these forces on the transport of bacteria in biochar/sand columns.

Compared to previous research, doping biochar with positive charges from ammonium and magnesium significantly improved its ability to attenuate microorganisms. Our results suggested that combining 2% of positively charged biochar 600 °C with sand was sufficient to reduce *E. coli* k12 by 46% and *E. coli* O157:H7 by 72%. Previously, we demonstrated that equivalent effects require at least 10% biochar mixed with sand [16]. The improved attenuation is likely due to improved interaction forces between the positively charged biochar and the negatively charged bacteria as shown by our DLVO analyses.

Our results emphasize the need to effectively monitor biochar functional classes to eliminate bacterial pollutants from contaminated water sources. Additionally, our data show that bacterial transport is strain-dependent and is mediated by interactions between bacterial functional groups and biochar and sand particle functional groups. With this in mind, efficient biochar filters should be adapted to specific applications, porous media types, ambient water chemistry, temperature, and microbial contaminants to be controlled.

Supplementary Materials: The following supporting information can be downloaded at: https://www.mdpi.com/article/10.3390/microbiolres14010018/s1, S1. Model bacterial cultures; S2. Biochar's Preparation, S3. Biochar's Characterization; S4. Physiochemical Characteristics of Sand; S5. Contact Angles Measurements and Modeling; S6. Interfacial free energy calculations; S7. Derjaguin, Landau, Verwey, and Overbeek (DLVO) theory of colloidal stability; Table S1: Physiochemical characteristics of sand; Table S2. Summary of the surface tension components of the propping liquids (mJ/m^2); Table S3: Contact angles of biochar, sand, and *E. coli* strains and the surface tensions and Hamaker constants (H_{132}) for *E. coli*/(biochar/sand) interactions in water; and Figure S1: Processed images of biochar different types pyrolyzed at (A–D) 400, 500, 600 and 700 °C, respectively and (E) sand. References [13–17,20,22,31,32] are cited in Supplementary Materials.

Author Contributions: Conceptualization, M.G.P. and N.I.A.-L.; methodology, all authors; software, N.I.A.-L. and K.Q.; validation, M.G.P. and N.I.A.-L.; formal analysis, all authors; investigation, all authors; resources, M.G.P. and N.I.A.-L.; data curation, K.Q. and S.H.M.; writing—original draft preparation, K.Q.; writing—review and editing, all authors; visualization, K.Q.; supervision, M.G.P. and N.I.A.-L.; project administration, M.G.P. and N.I.A.-L.; funding acquisition, M.G.P. and N.I.A.-L. All authors have read and agreed to the published version of the manuscript.

Institutional Review Board Statement: Not applicable.

Informed Consent Statement: Not applicable.

Data Availability Statement: Data shown here will be made available from the authors upon request, following the data restrictions employed by UTSA and WSU.

Conflicts of Interest: The authors declare no conflict of interest.

References

1. Mohanty, S.K.; Torkelson, A.A.; Dodd, H.; Nelson, K.L.; Boehm, A.B. Engineering solutions to improve the removal of fecal indicator bacteria by bioinfiltration systems during intermittent flow of stormwater. *Environ. Sci. Technol.* **2013**, *47*, 10791–10798. [CrossRef] [PubMed]
2. Mohanty, S.K.; Boehm, A.B. *Escherichia coli* removal in biochar-augmented biofilter: Effect of infiltration rate, initial bacterial concentration, biochar particle size, and presence of compost. *Environ. Sci. Technol.* **2014**, *48*, 11535–11542. [CrossRef]
3. Abbasi, B.; Ta, H.X.; Muhunthan, B.; Ramezanian, S.; Abu-Lail, N.; Kwon, T.-H. Modeling of permeability reduction in bioclogged porous sediments. *J. Geotech. Geoenvironmental Eng.* **2018**, *144*, 4018016. [CrossRef]
4. Anca-Couce, A. Reaction mechanisms and multi-scale modeling of lignocellulosic biomass pyrolysis. *Prog. Energy Combust. Sci.* **2016**, *53*, 41–79. [CrossRef]

5. Singh, G.; Lakhi, K.S.; Sil, S.; Bhosale, S.V.; Kim, I.; Albahily, K.; Vinu, A. Biomass derived porous carbon for CO_2 capture. *Carbon* **2019**, *148*, 164–186. [CrossRef]

6. Wang, K.; Brown, R.C.; Homsy, S.; Martinez, L.; Sidhu, S.S. Fast pyrolysis of microalgae remnants in a fluidized bed reactor for bio-oil and biochar production. *Bioresour. Technol.* **2013**, *127*, 494–499. [CrossRef] [PubMed]

7. Laird, D.A. The charcoal vision: A win–win–win scenario for simultaneously producing bioenergy, permanently sequestering carbon, while improving soil and water quality. *Agron. J.* **2008**, *100*, 178–181. [CrossRef]

8. Laird, D.A.; Brown, R.C.; Amonette, J.E.; Lehmann, J. Review of the pyrolysis platform for coproducing bio-oil and biochar. *Biofuels Bioprod. Biorefining* **2009**, *3*, 547–562. [CrossRef]

9. Abit, S.M.; Bolster, C.H.; Cai, P.; Walker, S.L. Influence of feedstock and pyrolysis temperature of biochar amendments on transport of *Escherichia coli* in saturated and unsaturated soil. *Environ. Sci. Technol.* **2012**, *46*, 8097–8105. [CrossRef]

10. Abit, S.M.; Bolster, C.H.; Cantrell, K.B.; Flores, J.Q.; Walker, S.L. Transport of *Escherichia coli*, *Salmonella typhimurium*, and microspheres in biochar-amended soils with different textures. *J. Environ. Qual.* **2014**, *43*, 371–388. [CrossRef]

11. Chung, J.W.; Foppen, J.W.; Izquierdo, M.; Lens, P.N. Removal of *Escherichia coli* from saturated sand columns supplemented with hydrochar produced from maize. *J. Environ. Qual.* **2014**, *43*, 2096–2103. [CrossRef]

12. Sasidharan, S.; Torkzaban, S.; Bradford, S.A.; Kookana, R.; Page, D.; Cook, P. Transport and retention of bacteria and viruses in biochar-amended sand. *Sci. Total Environ.* **2016**, *548*, 100–109. [CrossRef] [PubMed]

13. Abu-Lail, N.I.; Camesano, T.A. Specific and nonspecific interaction forces between *Escherichia coli* and silicon nitride, determined by Poisson statistical analysis. *Langmuir* **2006**, *22*, 7296–7301. [CrossRef] [PubMed]

14. Abu-Lail, N.I.; Camesano, T.A. The effect of solvent polarity on the molecular surface properties and adhesion of *Escherichia coli*. *Colloids Surf. B Biointerfaces* **2006**, *51*, 62–70. [CrossRef] [PubMed]

15. Park, B.-J.; Abu-Lail, N.I. The role of the pH conditions of growth on the bioadhesion of individual and lawns of pathogenic *Listeria monocytogenes* cells. *J. Colloid Interface Sci.* **2011**, *358*, 611–620. [CrossRef]

16. Suliman, W.; Harsh, J.B.; Fortuna, A.-M.; Garcia-Pérez, M.; Abu-Lail, N.I. Quantitative effects of biochar oxidation and pyrolysis temperature on the transport of pathogenic and nonpathogenic *Escherichia coli* in biochar-amended sand columns. *Environ. Sci. Technol.* **2017**, *51*, 5071–5081. [CrossRef]

17. Mood, S.H.; Ayiania, M.; Jefferson-Milan, Y.; Garcia-Perez, M. Nitrogen doped char from anaerobically digested fiber for phosphate removal in aqueous solutions. *Chemosphere* **2020**, *240*, 124889. [CrossRef]

18. Suliman, W.; Harsh, J.B.; Abu-Lail, N.I.; Fortuna, A.-M.; Dallmeyer, I.; Garcia-Perez, M. Influence of feedstock source and pyrolysis temperature on biochar bulk and surface properties. *Biomass Bioenergy* **2016**, *84*, 37–48. [CrossRef]

19. Smith, M.W.; Helms, G.; McEwen, J.-S.; Garcia-Perez, M. Effect of pyrolysis temperature on aromatic cluster size of cellulose char by quantitative multi cross-polarization 13C NMR with long range dipolar dephasing. *Carbon* **2017**, *116*, 210–222. [CrossRef]

20. Abu-Lail, N.I.; Camesano, T.A. Role of ionic strength on the relationship of biopolymer conformation, DLVO contributions, and steric interactions to bioadhesion of *Pseudomonas putida* KT2442. *Biomacromolecules* **2003**, *4*, 1000. [CrossRef]

21. Chen, G.; Zhu, H. Bacterial adhesion to silica sand as related to Gibbs energy variations. *Colloids Surf. B Biointerfaces* **2005**, *44*, 41–48. [CrossRef]

22. Van Oss, C.J. *Interfacial Forces in Aqueous Media*; CRC Press: Baton Rouge, LA, USA, 2006.

23. Vithanage, M.; Mayakaduwa, S.; Herath, I.; Ok, Y.S.; Mohan, D. Kinetics, thermodynamics and mechanistic studies of carbofuran removal using biochars from tea waste and rice husks. *Chemosphere* **2016**, *150*, 781–789. [CrossRef]

24. Ramezaniankeikanloo, S. Multiscale Investigations of the Effects of Chemical Stimuli on the Composition, Adhesion and Mechanics of *Pseudomonas putida* Cells and Biofilms. Ph.D. Thesis, Washington State University, Pullman, WA, USA, May 2018.

25. Afrooz, A.R.M.N.; Pitol, A.K.; Kitt, D.; Boehm, A.B. Role of microbial cell properties on bacterial pathogen and coliphage removal in biochar-modified stormwater biofilters. *Environ. Sci. Water Res. Technol.* **2018**, *4*, 2160–2169. [CrossRef]

26. Afrooz, A.N.; Boehm, A.B. *Escherichia coli* removal in biochar-modified biofilters: Effects of biofilm. *PLoS ONE* **2016**, *11*, e0167489. [CrossRef]

27. Hermansson, M. The DLVO theory in microbial adhesion. *Colloids Surf. B Biointerfaces* **1999**, *14*, 105–119. [CrossRef]

28. Xu, C.-Y.; Li, Q.-R.; Geng, Z.-C.; Hu, F.-N.; Zhao, S.-W. Surface properties and suspension stability of low-temperature pyrolyzed biochar nanoparticles: Effects of solution chemistry and feedstock sources. *Chemosphere* **2020**, *259*, 127510. [CrossRef]

29. Ramezanian, S.; Ta, H.X.; Muhunthan, B.; Abu-Lail, N. Role of ionic strength in the retention and initial attachment of *Pseudomonas putida* to quartz sand. *Biointerphases* **2018**, *13*, 041005. [CrossRef]

30. Van Oss, C.J. The forces involved in bioadhesion to flat surfaces and particles—Their determination and relative roles. *Biofouling* **1991**, *4*, 25–35. [CrossRef]

31. Dubinin, M.M. The equation of the characteristic curve of activated charcoal. *Dokl. Akad. Nauk. SSSR* **1947**, *55*, 327–329.

32. Dubinin, M.M.; Zaverina, E.D.; Radushkevich, L.V. Sorption and structure of active carbons. I. Adsorption of organic vapors. *Zhurnal Fiz. Khimii* **1947**, *21*, 151–162.